Glacier sliding, seismicity, and sediment entrainment

Bradley Paul LIPOVSKY[1], Colin R. MEYER[2], Lucas K. ZOET[3], Christine McCARTHY[4], Dougal D. HANSEN[3], Alan W. REMPEL[2], Florent GIMBERT[5]

[1]*Department of Earth and Planetary Sciences, Harvard University, Cambridge, MA, USA*

[2]*Department of Earth Sciences, University of Oregon, Eugene, OR, USA*

[3]*Department of Geoscience, University of Wisconsin–Madison, Madison, WI, USA*

[4] *Lamont-Doherty Earth Observatory, Columbia University, Palisades, NY, USA*

[5]*University of Grenoble Alpes, CNRS, IRD, Institut des Géosciences de l'Environnement (IGE), Grenoble, France*

Correspondence: Bradley Paul Lipovsky <brad_lipovsky@fas.harvard.edu>

ABSTRACT. The evolution of glaciers and ice sheets depends on processes in the subglacial environment. Shear seismicity along the ice–bed interface provides a window into these processes. Such seismicity requires a rapid loss of strength that is typically ascribed to rate-weakening friction, i.e., decreasing friction with sliding or sliding rate. Many friction experiments have investigated glacial materials at the temperate conditions typical of fast flowing glacier beds. To our knowledge, however, these studies have all found rate-strengthening friction. Here, we investigate the possibility that rate-weakening rock-on-rock friction between sediments frozen to the bottom of the glacier and the underlying water-saturated sediments or bedrock may be responsible for subglacial shear seismicity along temperate glacier beds. We test this 'entrainment-seismicity hypothesis' using targeted laboratory experiments and simple models of glacier sliding, seismicity, and sediment entrainment. These models suggest that sediment entrainment may be a necessary but not sufficient condition for the occurrence of basal shear seismicity. We propose that stagnation at the Whillans Ice Stream, West Antarctica may be caused by the growth of a frozen fringe of entrained sediment in the ice stream margins. Our results suggest that basal shear seismicity may indicate geomorphic activity.

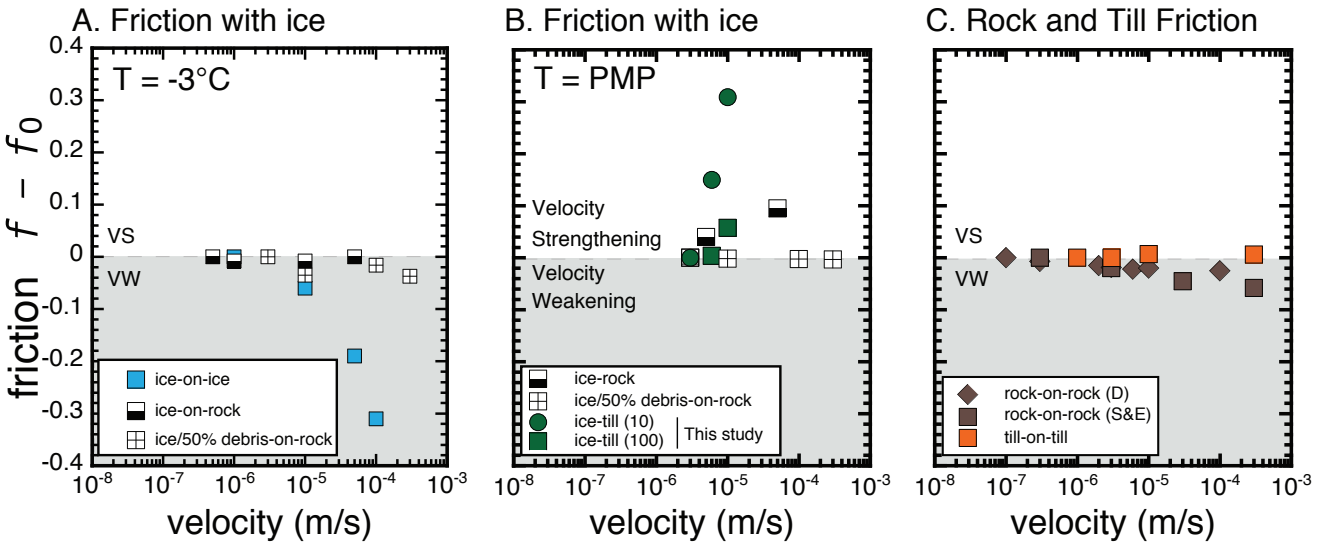

Fig. 1. A review of published and newly conducted laboratory friction experiments on glacial materials. A. Experiments conducted at -3C involving ice, B. experiments conducted at the pressure-melting point involving ice, and C. experiments involving rock and till only. The data sources used in this figure are listed in Table 1.

INTRODUCTION

The resistive stresses generated during glacier sliding tend to slow down ice motion and therefore favor glacier growth and stability (van der Veen and Whillans, 1989). Many processes govern this resistance to sliding (Clarke, 2005). Given the inherent spatial limitations associated with borehole or other direct access to the subglacial environment, geophysical methods such as seismology often provide the most feasible avenue of investigation at the glacier synoptic scale (Podolskiy and Walter, 2016; Aster and Winberry, 2017). Although a wide variety of naturally occurring phenomena may generate seismic waves in glaciers, basal stick-slip shear motion is particularly informative of glacier sliding processes (Zoet and others, 2012; Winberry and others, 2013; Allstadt and Malone, 2014; Helmstetter and others, 2015; Barcheck and others, 2018). However, despite the commonplace occurrence of this type of seismicity, several basic questions remain concerning its underlying mechanical origin.

Shearing motion that is sufficiently fast to generate seismic waves requires a rapid loss of strength along a sliding interface. Such a strength loss may occur when a sliding interface experiences less friction at greater amounts of sliding or sliding rate. Sliding interfaces are said to have velocity weakening friction.

The degree to which rate-weakening occurs is quantified through the parameter (Rice and Ruina, 1983),

$$(b-a) \equiv -v\frac{\mathrm{d}f_{ss}(v)}{\mathrm{d}v}, \tag{1}$$

where $f_{ss}(v)$ denotes the steady state friction coefficient f_{ss} is a function of the sliding velocity v. The exact nature of sliding interfaces in glacial materials has been scrutinized by numerous laboratory studies which have examined the sliding of both clean and debris-laden ice in contact with ice, rock, and till (Table 1). These studies, however, have generally failed to reproduce the rate-weakening friction necessary to explain basal seismicity under temperate sliding conditions (Figure 1).

We focus on temperate sliding conditions, i.e., glaciers with basal ice that is at the pressure-melting point (PMP). Such conditions characterize most fast flowing glaciers and ice streams (Clarke, 2005). Fast flowing glaciers that rest on water-saturated sediment may have basal ice that infiltrates some distance into the sediment. This region of ice infiltration is referred to as a frozen fringe. Perturbations to the basal thermal state are expected to alter the thickness of this fringe while maintaining an ice-water interface at the pressure-melting point (Rempel, 2008). For this reason, temperate conditions are expected to prevail along the basal sliding interface of fast flowing glaciers and ice streams, a prediction which is readily confirmed using direct borehole observation (Kamb, 2001).

Numerous studies report basal shear seismicity along temperate glacier beds. Location accuracy varies substantially between studies and is sometimes not reported at all. One such high resolution study by Canassy and others (2016) estimates a seismicity location accuracy of 2.5 to 5.1 m. This study was able to achieve particularly high accuracy because of a coincident tomographically-derived velocity model. A typical temperature gradient 0.02°C/m (Kamb, 2001) then suggests that these events could have spanned a region with a temperature difference of about 0.05 to 0.10°C from the temperate glacier bed. Other studies with lower quality velocity models have found somewhat lower accuracy. In Greenland, Roeoesli and others (2016) estimate seismicity location accuracy of 25 m and on Antarctic ice streams, Anandakrishnan and Bentley (1993) and Smith and others (2015) estimate seismicity location accuracy of 10 m and 37 m, respectively. We interpret these observations to be consistent with shear seismicity occurring under temperate conditions.

Temperate conditions, however, pose a paradox in terms of basal shear seismicity. Despite the above-described occurrence of seismicity in this environment, we are aware of no laboratory study to date that has found rate-weakening behavior in material combinations that involve water ice at its pressure-melting

point sliding against sediments. Till-on-till, ice-on-till, and ice-on-ice sliding, for example, have been shown to exhibit rate-strengthening friction under temperate conditions (Barnes and others, 1971; Oksanen and Keinonen, 1982; McCarthy and others, 2017). Rock-on-rock sliding, however, commonly exhibits rate-weakening behavior (see reviews by Marone, 1998; Scholz, 1998; Dieterich, 2007).

We therefore propose the 'entrainment-seismicity hypothesis' that shear seismicity along temperate glacier beds is caused by the sliding of ice with entrained debris against underlying sediments or bedrock. This hypothesis is illustrated schematically in Figure 2. The main goal of this study is to evaluate the 'entrainment-seismicity hypothesis' as well as several competing hypotheses.

Under some circumstances, moderately rate strengthening friction may also be able to generate rapid weakening. In particular, rapid shearing motion due to sliding instability is possible between elastically dissimilar solids when $(a - b)$ is smaller than a threshold value (Rice and others, 2001). While such a mechanism may permit shear seismicity in the sliding of ice with high deris content-on-rock ($a-b \approx 0.0005$), it seems unlikely to explain other material pairs shown in Figure 1 which have much stronger velocity strengthening ($a - b$ as large as 0.131). We discuss this point, as well as other competing hypotheses, in the subsection titled *Competing hypotheses*.

This paper is organized as follows. We first use laboratory experiments to evaluate the possibility that ice-on-till friction is rate-weakening at the pressure melting point, a competing hypothesis. Then, in order to better understand the conditions under which entrainment and seisimicity may co-occur, we develop simple physical models of these processes. These models confirm that seismicity and sediment entrainment are both expected to occur at high effective pressures relative to certain thresholds. We conclude by discussing additional competing hypotheses, the relationship between basal shear seismicity and bed shear stress, and the role of sediment entrainment in the stagnation of the Whillans Ice Stream. Available data at the present time support the 'entrainment-seismicity hypothesis' over competing hypotheses regarding the origin of subglacial shear slip seismicity along temperate glacier beds. This result suggests that basal shear seismicity may be used to infer subglacial geomorphic activity.

LABORATORY SLIDING EXPERIMENTS

The frequent synchronous occurrence of both glacial till (Alley and others, 1986) and basal shear seismicity (Anandakrishnan and Bentley, 1993) beneath fast-flowing temperate-bed glaciers, prompts us to investigate frictional sliding between ice and till. In this section, we describe an exploratory study of velocity stepping

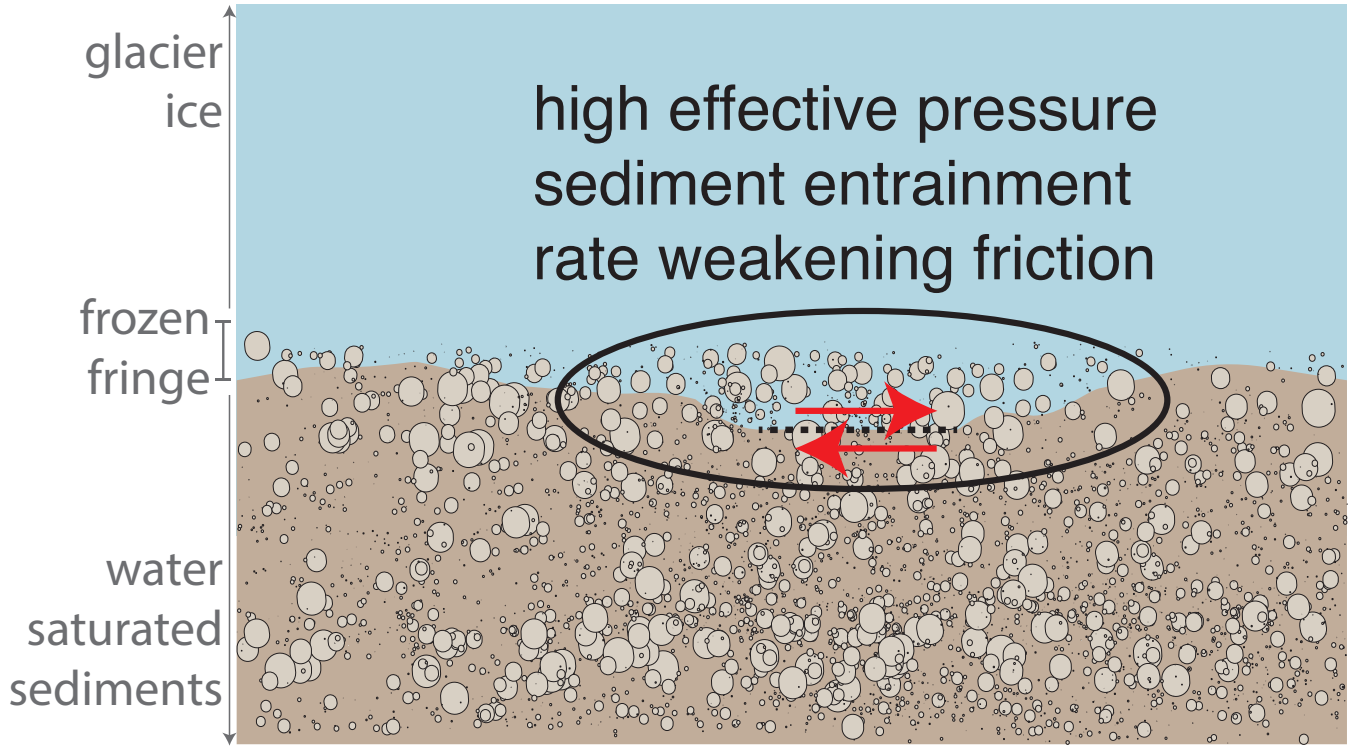

Fig. 2. Basal shear seismicity in temperate glaciers is expected to be caused by rock-on-rock friction as entrained sediments slide across the underlying water saturated sediments or bedrock. The red arrows indicate relative motion and the black oval indicates a region with locally elevated effective pressure and therefore locally thickened frozen fringe.

tests designed to specifically explore the rate behavior of an ice-till interface at temperate conditions. Although the healing process has been investigated for temperate ice slid over till (Zoet and Iverson, 2018), to our knowledge no laboratory experiments on the transient friction response have been reported with this pairing of materials.

Experimental methods

A direct shear apparatus was used to slide a 10×10×3 cm block of temperate ice over a 10×10×1 cm thick layer of saturated till for a total displacement of ∼1 cm (Figure 3). The device was housed in a cold room that was held at 0 ± 0.5° C. The apparatus consisted of a modified version of a shear box produced by ELE International and was sufficiently stiff to perform velocity stepping experiments. Weights hung from a lever arm applied a vertical load to the top of the sample chamber, which could expand or contract during shear to accommodate sample dilation or contraction. A load cell oriented perpendicular to vertical motion measured shear stress, and two linear variable displacement transducers (LVDTs) recorded horizontal displacement of the sample chamber and vertical displacement of the top platen. A bronze porous plate was placed at the base of the sample chamber to allow melt water to drain from the till.

We used till from the Ozaukee member of the Kewaunee formation in all experiments. This unit is comprised of approximately 13% sand, 47% silt, and 40% clay. The lithology is 50 to 63% illite, and ∼20% kaolinite plus chlorite (Acomb and others, 1982). Grains larger than 1/10 the minimum sample chamber dimension were removed from the sample in order to avoid any length scale effects. The ice sample was constructed from deionized (DI) water that was frozen, crushed, and sieved to obtain a mixture of randomly oriented grains with diameters ranging from 2-6 mm. Ice grains were then layered in the sample chamber, void space was filled with DI water, and the assemblage was frozen. The till was allowed to reach thermal equilibrium in the cold room, and a GEC (brand name) temperature probe with greater than 0.01° C temperature accuracy was embedded ∼ 1 cm into the bottom surface of the ice block to ensure that temperatures reached the pressure-melting point prior to shear.

Once ice and till reached the pressure-melting point, the temperature probe was removed, the sample chamber was placed in the direct shear apparatus, and the horizontal driving ram was immediately engaged to initiate shearing. This immediate shearing and the short duration of the experiments prevented the growth of a frozen fringe layer at the base of the ice block. Minimal melting occurred over the ∼ 10 min duration of each experiment. The short duration and visual inspection of the sample following the exper-

iment ensured that debris-free ice was slid over the till unit, thereby elucidating the rate-strengthening effect for the end member case of clean, temperate ice sliding over saturated till.

Two experiments were conducted, one at an applied normal stress of 10 kPa and another at 100 kPa. An example time series of the resulting shear stress evolution is shown in the Figure 3a. Three velocity steps of 3–6, 6–10, and 10–30 μm/s were imposed in each experiment. Sliding was initiated at 3 μm/s. Once the measured shear stress reached a steady state, the velocity was increased.

Experimental results

In both experiments, all velocity steps resulted in an increase in frictional resistance in response to a sudden change in sliding rate (Figure 1). The frictional resistance to increased sliding rate at 10 kPa normal stress (Figure 3a). A 3–6, 6–10, and 10–30 μm/s, increase in slip speed resulted in $a - b$ values of 0.145, 0.137, 0.110 at 10 kPa normal stress, and $a-b$ values of 0.001, 0.015, 0.052 at 100 kPa, respectively. All $a-b$ values are positive, indicating that debris-free temperate ice slid over a saturated till leads to a rate-strengthening behavior in response to a sudden increase in slip speed.

The degree of strengthening compared to other systems is also demonstrated in Figure 1, which shows steady state friction as a function of velocity, normalized by a low velocity reference point. Only those systems plotting within the gray region display rate-weakening behavior. The details of our experimental measurements are listed side-by-side with several previous studies in the Supplementary Materials. For comparison, results from a rate weakening biaxial test by Zoet and others (2013) are shown in Figure 3c and d.

SIMPLE MODELS OF SEISMICITY AND ENTRAINMENT

We now present simplified models of basal sliding, seismicity, and sediment entrainment. The purpose of these simulations is to test the 'entrainment-seismicity hypothesis' by verifying whether it is possible for seismicity to happen at the same time as sediment entrainment. We find that this is indeed the case because both sediment entrainment and seismicity require high effective pressure $N \equiv p_i - p_w$, with ice pressure p_i and water pressure p_w. Specifically, if effective pressures are too low then frictional weakening never becomes sufficiently pronounced to create stick-slip seismicity. Similarly, if effective pressures are too low then ice will not penetrate into the underlying sediments and sliding will occur with debris-free ice sliding along the water-saturated substrate.

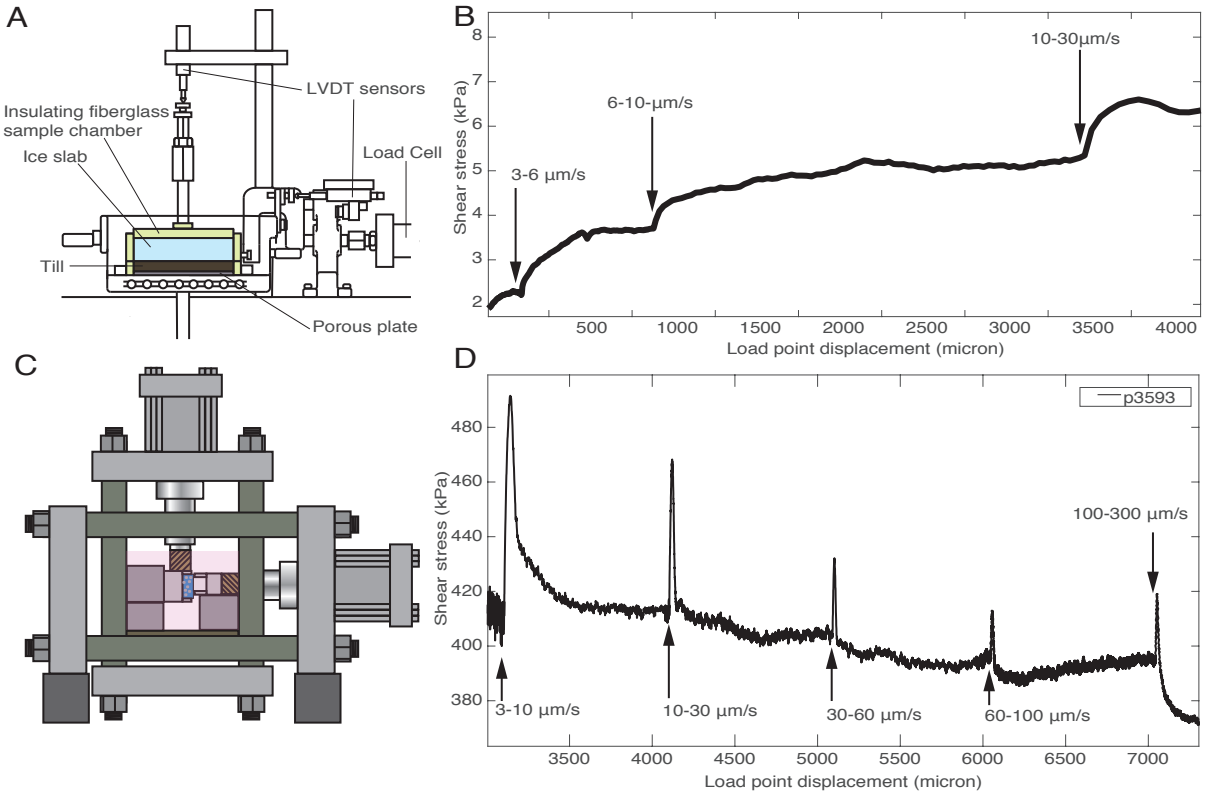

Fig. 3. Diagrams of our experimental apparatus (A. and C.) and representative sliding histories during velocity stepping experiments (B. and D.). The sliding velocities are annotated throughout each shear stress-versus-slip plot. The two experiments show increasing (B.) and decreasing (D.) friction as a function of sliding velocity. These experiments have ice-on-till at the pressure melting point (A and B.) and ice with 50% debris content-on-rock at -3°C by Zoet and others (2013) (C and D.). The two apparatus used correspond to the ELE direct shear mechanism (A.) and a biaxial testing apparatus with double-direct shear configuration (C). In both cases the sample is show in blue, but note that the test specimen in (A.) is 10 cm long whereas the specimen in (C.) is 7 cm long.

Table 1. Table of laboratory friction studies

Study	Materials	Temperature	Response type
Kennedy and others (2000)	ice-on-ice	-3	rate-weakening
McCarthy and others (2017)	ice-on-rock	-3	rate-strengthening
Zoet and others (2013)	ice/50%till-on-rock	-3	rate-weakening
This study	ice-on-till (N=10 kPa)	PMP	rate-strengthening
This study	ice-on-till (N=100 kPa)	PMP	rate-strengthening
Zoet and others (2013)	ice/50%till-on-rock	PMP	mildy rate-strengthening
McCarthy and others (2017)	ice-on-rock	PMP	rate-strengthening
Rathbun and others (2008)	till-on-till	ambient	rate-strengthening
Scholz and Engelder (1976)	rock-on-rock	ambient	rate-weakening
Dieterich (1978)	rock-on-rock	ambient	rate-weakening

The simple models that we present here are consistent with sediment entrainment being a necessary but not sufficient condition for subglacial seismicity. Entrainment, under the 'entrainment-seismicity hypothesis', is necessary insofar as it results in a rate-weakening, rock-on-rock interface. We begin this section by describing an additional necessary condition for seismicity.

Seismicity and frictional sliding

We begin by describing a simple model of frictional sliding to quantify the conditions under which stick-slip motion is expected to occur. We make use of rate-and-state friction as a constitutive law for the basal sliding interface. This type of sliding law is commonly used to model stick-slip behavior (Scholz, 1998; Marone, 1998; Dieterich, 2007). Rate-and-state friction describes two phenomena associated with the friction coefficient f, defined as the ratio of shear stress τ to effective pressure N. These two behaviors, described elsewhere in detail (Rice and others, 2001), consist of a rate-dependent transient during a step in loading velocity followed by a subsequent evolution to a steady state. So-called rate-weakening materials have a steady state friction coefficient that is a decreasing function of loading rate. Importantly, rate-weakening materials are conditionally stable, meaning that they may exhibit stick-slip motion if certain additional criteria are met. Specifically, seismicity occurs when the effective pressure exceeds a critical value (Rice and others, 2001),

$$N_c \equiv \frac{kL}{b-a} \tag{2}$$

for seismogenic patch rigidity k, rate-weakening parameter $b-a$ (Equation 1), and state evolution distance L. These parameters are discussed in detail by Lipovsky and Dunham (2016) and Lipovsky and Dunham (2017). As an example of typical values, we note that if $k = 10$ MPa/m, $b - a = 0.01$ and $L = 10$ μm, then seismicity is expected to be possible only when the effective pressure is greater than 10 kPa. We note that the state evolution distance L is often inferred to vary with the size of the sliding region; our choice of a relatively small value in this example calculation is typical of $\sim$ meter-scale sliding regions (Lipovsky and Dunham, 2016). Lastly, we note that dynamic variations in normal stress (Linker and Dieterich, 1992; Selvadurai and others, 2018) and stiffness (Leeman and others, 2015) are both neglected here in order to focus on the most basic relationship between friction and entrainment.

Sediment entrainment

We next turn to a simple model of sediment entrainment. The way in which sediments are entrained depends on the forces exerted on the sediments, the heat fluxes into and out of the sediment, and water flow through the sediments. In the subglacial environment, the overburden weight of the overlying ice presses the ice against the underlying till sediments. The water pressure resists some of the weight of the ice but the difference in pressures (i.e. the effective pressure N) causes the ice to conform to the shape of the sediments. Locally, this requires very high curvature on the sediment grain scale, leading to curvature-induced premelting (Rempel and others, 2001, 2004; Dash and others, 2006). When the effective pressure is large enough, the ice can infiltrate into the sediments and form a partially frozen region known as a frozen fringe (O'Neill and Miller, 1985). Thus, similar to the frictional onset of stick-slip, sediment entrainment is expected to occur at high effective pressure (Rempel, 2007, 2008, 2009a,b). The critical effective pressure for ice to infiltrate into a granular substrate is approximated by (Meyer and others, 2018a),

$$N_f \equiv 2\gamma/r, \tag{3}$$

for surface energy $\gamma \approx 0.035$ J/m^2 and subglacial sediment grain size r. For the clay rich tills found on the Siple Coast ice streams, micron-scale grain sizes give an estimate of the critical effective pressure to be in the range of several tens of kPa, for example, 70 kPa for 1 μm grains or 7 kPa for 10 μm grains. In this way, glaciers entrain large quantities of sediment, which are expected to affect the rate and character of their sliding as well as the occurrence of basal seismicity.

The effect of debris content

As the fraction of entrained debris increases, we expect that the frictional properties of the ice–bed interface will begin to resemble those of rock-on-rock friction. This transition occurs at roughly 50% ice volume fraction (Moore, 2014) but also depends on grain size (Emerson and Rempel, 2007). Equation 3 is therefore consistent with the notion that high effective pressure is a requirement for stick-slip motion. In particular Equation 3 states that effective pressures must be great enough to entrain debris along the interface.

As a caveat, we note that frictional resistance may transition before the condition of Equation 3. Even without fully encapsulating obstacles, for example, ice could drag the top layer of particles against their lower neighbors. Since this behaviour would still require enough conformity between the ice and particle surfaces, it ought to nevertheless involve some sort of threshold-like transition. Because our main goal is to capture the existence of such a transition, we retain the condition given by Equation 3.

The effect of the viscous flow of ice

To ellucidate the role of viscous flow in the overlying ice, we present a simplified model that incorporates the coupled effects of viscoelasticity and frictional sliding in Appendix A. This approach is a simplification of other viscoelastic models that resolve the basal earthquake cycle (Goldberg and others, 2014). The most important result is that viscous deformation overwhelms stick-slip motion when the Maxwell time is much less than the earthquake recurrence time. This behavior is an extension of the elastic case, where stick-slip motion occurs when weakening exceeds the increase in elastic stress per unit slip (Rice and Ruina, 1983). For the viscoelastic case, effective pressures may become sufficiently large that viscous deformation in the ice overwhelms stick-slip motion. This occurs when

$$N > N_c \left(1 - \frac{T_r}{T_m}\right)^{-1}. \tag{4}$$

where $T_m \equiv \mu/k$ is the Maxwell time with linear ice viscosity μ, T_r is a time scale that is proportional to the stick-slip recurrence time of an equivalent elastic system (i.e., with $\mu \to \infty$), and we have used N_c from Equation 2. We note that the results discussed in this section only strictly pertain to the linear, near-stable conditions considered in Appendix A. We currently have ongoing work in this area that will examine the full nonlinear system. However, based on prior experience (Lipovsky and Dunham, 2016, 2017), we nevertheless expect the linear problem to yield useful insights.

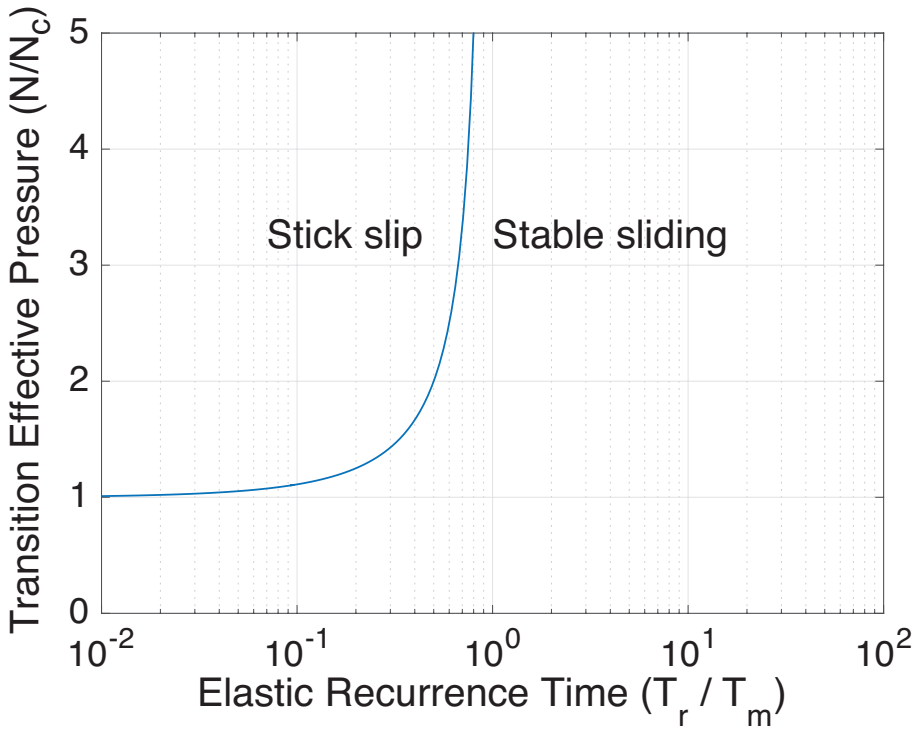

Fig. 4. Under a viscoelastic ice rheology, stick-slip motion cannot occur when the stick-slip recurrence time of the equivalent elastic system T_r is equal to the Maxwell viscoelastic relaxation time. As this condition is approached, the effective pressure required for stick-slip motion diverges.

Equation 4 emphasizes that viscous effects become important as the recurrence time approaches the Maxwell time (Figure 4). Stick-slip events are not expected to occur when the stick-slip recurrence time is greater than the Maxwell time. This condition could alternatively be written in terms of a critical value of any system parameter. In terms of a critical sliding velocity,

$$v_c = \frac{a}{b-a}\frac{Lk}{\mu}. \tag{5}$$

Equations 4 and 5 are different ways of stating the same idea: that the stick slip instability vanishes at a critical point of the underlying dynamical system. These two expressions are connected because the recurrence time scales inversely with the loading rate $T_r \sim 1/v_0$, so that at low loading rates v_0, viscous stabilization occurs. These findings are also consistent with more detailed continuum models of stick-slip cycles in viscoelastic media (Allison and Dunham, 2018).

Our analysis predicts that effective pressures may become sufficiently large that viscous deformation overwhelms stick-slip motion. This occurs because the recurrence time depends on effective pressure but the Maxwell time does not. As a result, seismicity may be extinguished in the deep interior of ice sheets. This prediction may be tested by future ice sheet seismicity location studies.

In Figure 5, we show how viscosity limits the tenable shear stress for hard and soft beds. This figure shows that viscous flow is particularly important for glaciers resting on bedrock with high shear modulus as opposed to glaciers resting on sediment with lower shear modulus. In each of these figures, seismicity is expected to occur due to stick-slip motion for all conditions represented by points above the blue curves. We note that seismicity generally occurs at high shear stresses, consistent with earlier results connecting glacier bed shear stress to glacier bed seismicity (Alley and others, 1994).

Viscous flow imposes another necessary condition for seismicity. Specifically, Equation 4 (or, equivalently, Equation 5) must be satisfied. Figure 5 shows that this condition poses a more severe limitation when the glacier bed has a shear modulus typical of unbroken bedrock. In this case, a glaciologically uncommon (Morlighem and others, 2013; Meyer and others, 2018a) combination of high bed shear stress (>200 kPa) and high sliding velocities (>2 km/a) are required to cause basal seismicity. We revisit implications of this finding in the discussion section.

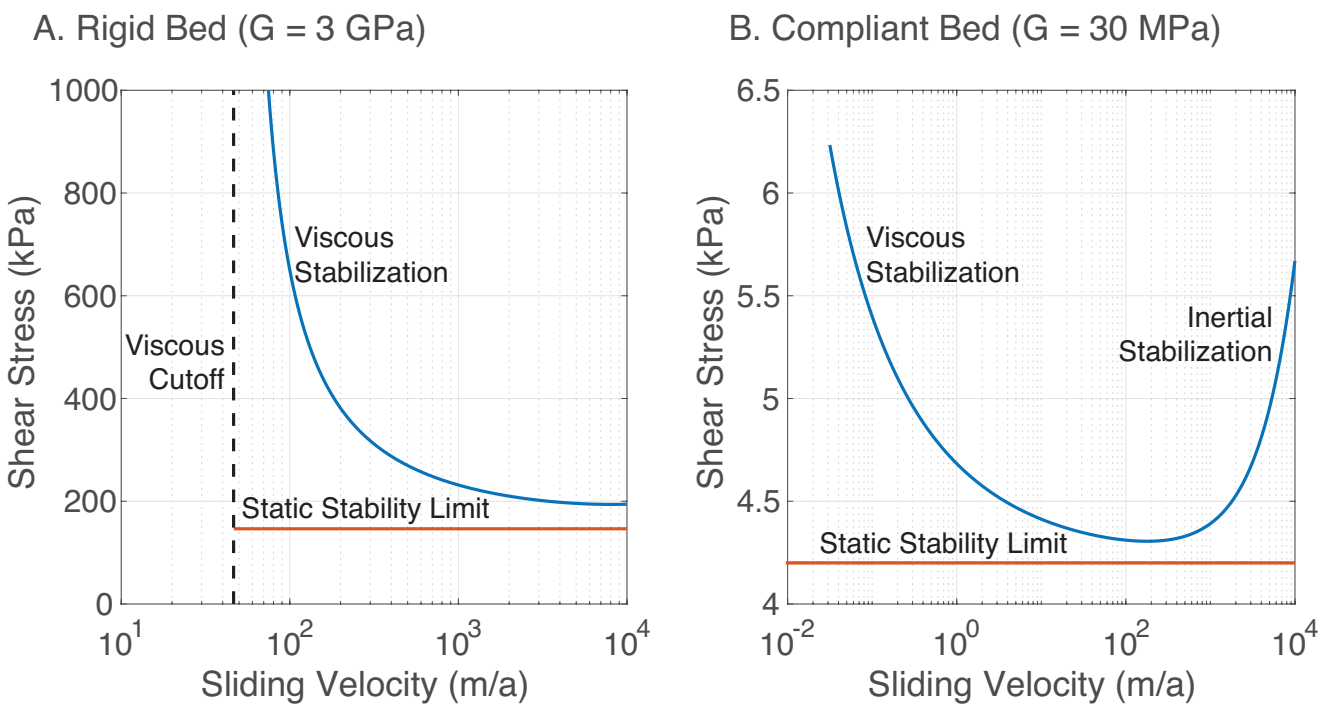

Fig. 5. Stability diagrams where stick-slip seismicity occurs at conditions represented by points above the blue curves. The blue lines denote neutral stability curves; they follow values where shear stress $\tau = fN$ takes critical value. The two panels show the cases of hard (A) and soft (B) beds.

Table 2. Table of parameters

Quantity	Symbol	Unit	Value
Hard Bed Ice shear modulus	G	GPa	30
Soft Bed Ice shear modulus	G	GPa	0.03
Radiation damping parameter	η	MPa/(m/s)	0.11
Bed obstacle dimension	R	m	1
Bed obstacle aspect ratio	ϵ		0.01
Nominal friction coefficient	f_0		0.4
Direct effect parameter	a		5×10^{-3}
Healing parameter	b		15×10^{-3}
State evolution distance	L	μm	1

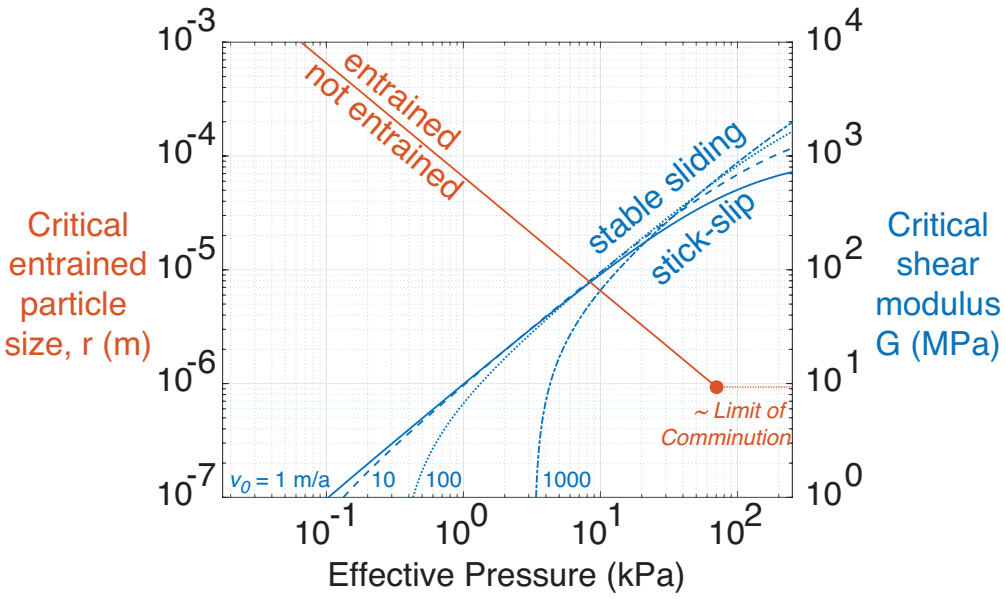

Fig. 6. Basal stick-slip seismicity requires sufficiently high effective pressure ($N > N_c$) so as to entrain almost all grain sizes down to the micron scale. The comminution limit is on the order of 1 μm (Sammis and Ben-Zion, 2008; Meyer and others, 2018a).

DISCUSSION

Our central hypothesis is that sediment entrainment is responsible for subglacial shear slip seismicity. Using the models derived in the previous section, we illustrate the necessary conditions for stick-slip motion and sediment entrainment in Figure 6. This figure illustrates that the effective pressure limitation of seismicity is expected to be much more common than effective pressure limitation of sediment entrainment. Specifically, entrainment of some grain size is possible at any N, with only the smallest entrained grain size varying. Seismicity, in contrast, is inhibited at low effective pressures.

Before continuing on to discuss several testable predictions of our proposed relationship between sediment entrainment and basal seismicity, we first discuss several competing hypotheses.

Competing hypotheses

Ice-on-ice friction

One competing hypothesis holds that subglacial shear seismicity in temperate glaciers could be caused by ice-on-ice friction. This alternative hypothesis is problematic, however, for several reasons. Foremost among these reasons is that, to our knowledge, the preliminary body of work reporting on laboratory friction

experiments in an ice-ice configuration, at the pressure melting point, has yet to observe rate-weakening behavior. Although Kennedy and others (2000) and Maeno and Arakawa (2004) report rate-weakening at temperatures as warm as -3C$^\circ$ and -10C$^\circ$, such cold temperatures are unlikely to be representative of behavior at the pressure-melting point (Barnes and others, 1971).

It is furthermore difficult to invoke ice-on-ice friction for the reason that deformation in the subglacial environment is typically thought to be localized to a narrow sliding plane at the interface between ice (perhaps with entrained sediments) and the underlying bedrock or sediments. Such behavior was demonstrated experimentally by (Zoet and Iverson, 2018). Glacier thrust faulting is a possible exception to this statement which we discuss later. With regards to basal sliding, however, borehole observations consistently have shown that deformation in the subglacial environment of fast flowing, temperate bed glaciers is narrowly localized along the ice-sediment interface (Blake and others, 1994; Kamb, 2001). This localization is expected because high water pressures lower frictional strength at the ice–sediment interface but not within the ice.

Glacier thrust faulting is thought to sometimes occur along a sliding interface located entirely within the ice. This phenomenon was reviewed by Moore and others (2010), who concluded that the 1983 surge of the Variegated Glacier constitutes the only known case of unambiguous thrust faulting. From this assessment, it would not appear as if glacier thrust faulting is a sufficiently pervasive phenomenon to describe the widespread occurrence of subglacial shear seismicity. Furthermore, many thrust faults are identified by the presence of entrained basal debris, thus suggesting that sediment entrainment may play a role in these structures as well (Lovell and others, 2015). Even if such fractures were somehow formed between ice surfaces near the pressure melting point, we would expect them to sinter and heal (Hosler and others, 1957).

Particle ploughing and cavitation

Particle ploughing (Tulaczyk and others, 2001; Moore and Iverson, 2002; Thomason and Iverson, 2008; Iverson, 2010) and cavitation (Schoof, 2005; Zoet and Iverson, 2015, 2016) both give rise to rate-weakening behavior. While it seems plausible that the transmission of contact forces during particle ploughing could largely be an elastic process that is relevant to glacier stick-slip seismicity, this seems unlikely to be the case for cavitation, a mostly viscous process. The effect of particle ploughing, however, was probably minimized in our experiment by removing clasts larger than 1/10 of the smallest specimen diameter. Experiments on

larger samples would clarify the potential seismogenic role for particle ploughing.

Thermal weakening due to shear heating

Shear heating can weaken frictional interfaces when sliding occurs at high enough velocity and for a long enough duration to cause the formation of a lubricating water layer (Barnes and others, 1971; Kennedy and others, 2000; Rice, 2006; Rempel and Rice, 2006; Viesca and Garagash, 2015). Such an explanation in fact appears as an early proposed mechanism for glacier stick-slip motion (Robin, 1976). Ice-on-rock friction experiments show that substantial weakening requires that the bulk solid temperature be below the pressure-melting point. At the pressure-melting point, shear heating does not appear to cause weakening but instead results in a net strengthening of the interface (Barnes and others, 1971), perhaps due to the enlargement of asperity contact areas. Given our focus on temperate conditions at the pressure-melting point, this line of reasoning seems to preclude a significant role for shear heating as a mechanism for generating rate-weakening behavior.

Elastic bimaterial instability

Rice and others (2001) demonstrated that mildly rate strengthening friction may be unstable to perturbations due to an elastic coupling between sliding and effective pressure. This result probably does not apply to our experiments because of the large $a - b$ values measured, particularly at 10 kPa effective stress ($a - b = 0.131$). Bimaterial instability could, however, conceivably destabilize the moderately rate strengthening friction measured by Zoet and others (2013) in the sliding of debris laden ice against rock ($a - b \approx 0.0005$). Quantifying this effect, however, requires knowledge of parameters measured under variable normal stress and such parameters were not measured by Zoet and others (2013). In lieu of such measurements, we simply note here that the potentially unstable, moderately strengthening friction measured by Zoet and others (2013) is consistent with the 'entrainment-seismicity hypothesis' in so far as it suggests that seismicity is possible when debris-laden ice slides against rock. Furthermore, the measurements made by Zoet and others (2013) may reflect a transitional case between rate strengthening and weakening behavior, as their 50% weight fraction debris is lower than the 50% volume fraction where rock-on-rock friction is expected to dominate the rheological response (Moore, 2014).

Sediment entrainment and deceleration of the Whillans Ice Stream

We expect our analysis of glacier sliding seismicity to be generally applicable to any glacier and ice sheet. However, given the richness of observations from the Siple Coast region of Antarctica, we now discuss our results in the context of the Siple Coast ice streams. We specifically focus on the Whillans Ice Stream (WIS), a fast flowing ice stream that is currently undergoing a decades-long deceleration (Beem and others, 2014), while simultaneously suffering large-scale stick-slip motion (Bindschadler and others, 2003; Wiens and others, 2008; Winberry and others, 2011; Pratt and others, 2014).

Lipovsky and Dunham (2017) found that spatially heterogeneous rate-strengthening and rate-weakening friction were required in order to match GPS observations of individual slip events on the WIS. In particular, the central part of the WIS was found to be rate-strengthening while the margins were rate-weakening. In terms of the proposed relationship between seismicity and sediment entrainment, we reinterpret the findings of Lipovsky and Dunham (2017) to suggest that sediment entrainment is currently taking place in the margins of the WIS. Lipovsky and Dunham (2017) estimate subglacial effective pressure to be 28 kPa. This number is consistent with direct hydraulic head measurements (Kamb, 2001), although the latter show a wide variation. Using this estimate of effective pressure and Equation 3 suggests that under present conditions, grain sizes as small as 2.5 μm may be entrained.

We propose WIS stagnation is being driven by the growth of a frozen fringe in the ice stream margins. This hypothesis is consistent with declining water pressure, as originally proposed by Alley and others (1994) and plausibly related to the subglacial hydrology in the vicinity of active shear margins (Meyer and others, 2018b; Meyer and Minchew, 2018). The growth of a frozen fringe is expected to ultimately decelerate ice flow by creating a large anchor of frozen sediments with extreme resistance to sliding (Meyer and others, 2018a). While we do not model this entire process here, in the next section we examine several simplified simulations that illustrate the mechanics of fringe growth.

Fringe thickness simulations

To test the idea that sediment entrainment is linked to the increased basal seismicity and attendant slowing of the Whillans Ice Plain (WIS), we ran a series of simulations of transient frozen fringe growth under conditions similar to WIS (Figure 7). The numerical calculations underlying our simulations are described by Rempel (2007, 2008). The inputs into the simulations are the effective pressure N, the geothermal heat flux Q_g, the conductive heat flux into the overlying ice Q_b, and the frictional heat generated at the basal

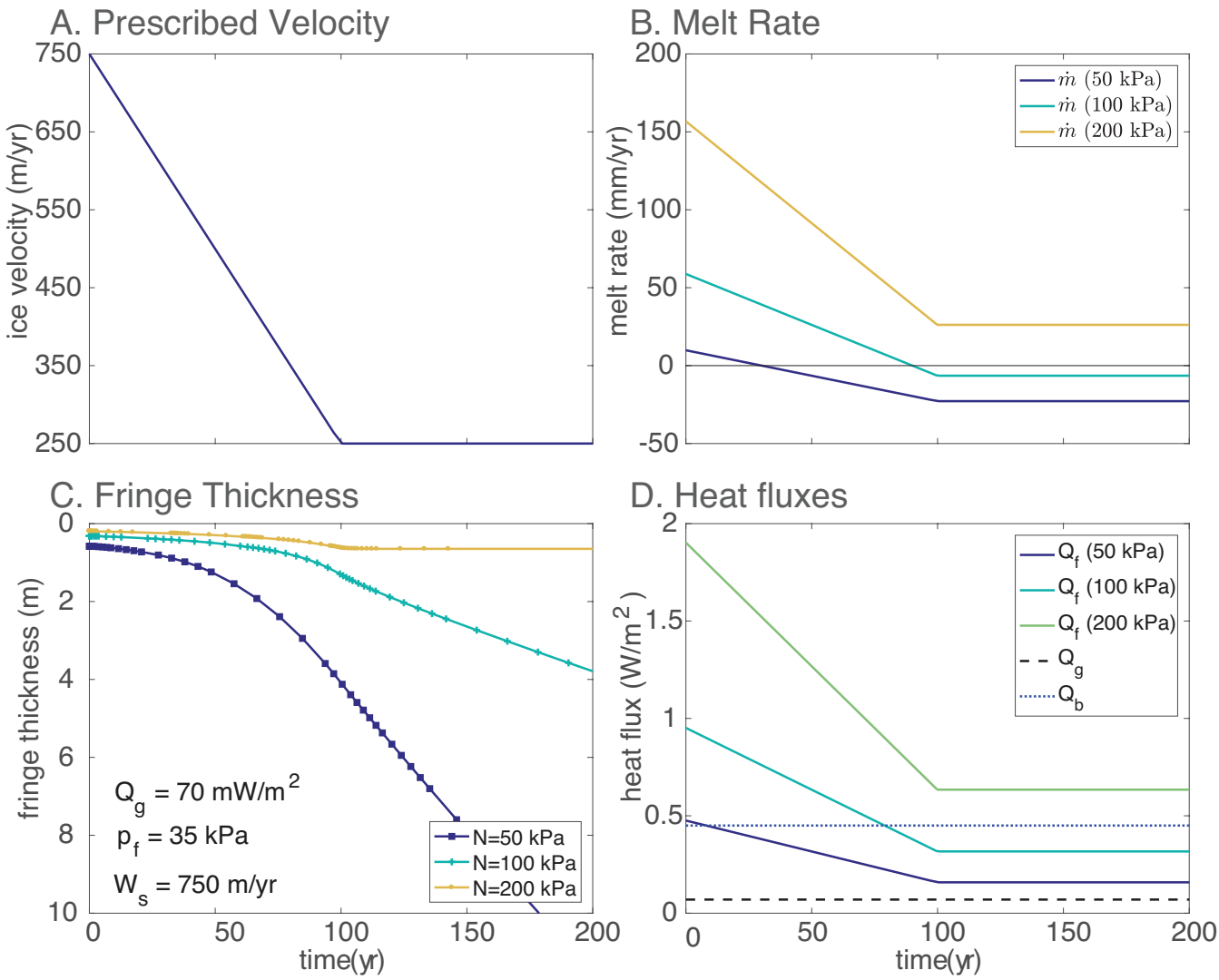

Fig. 7. Transient fringe evolution at the Whillans Ice Plain (WIS): (A) prescribed ice sliding velocity showing the WIS slowdown, (B) basal melt rate for three values of the effective pressure, (C) fringe thickness as a function of time for three effective pressures. Only the largest effective pressure approaches a steady state an the the other two grow with time, (D) prescribed heat fluxes with variation in velocity and effective pressure.

interface Q_f. The basal melt rate $\dot{m}$ is then

$$\rho_i \mathscr{L} \dot{m} = Q_g + Q_f - Q_b, \tag{6}$$

where ρ_i is the ice density, $\mathscr{L}$ is the latent heat. The frictional heat Q_f is given as

$$Q_f = \mu N W_s, \tag{7}$$

with the coefficient of friction μ and the sliding velocity W_s. Consistent with the observed slowing of WIS (Beem and others, 2014), we prescribe a sliding velocity that starts at 750 m/yr and slows to 250 m/year over 100 years (Figure 7a). This translates into the frictional heat fluxes given in Figure 7d for the different values of the effective pressure. We choose the conductive loss $Q_b = 0.45$ W/m^2 so that when we compile the heat fluxes into the melt rate by Equation 6 there is a transition from net melting to net freezing as WIS slows.

As shown in Meyer and others (2018a), the fringe thickness is determined by the magnitude of the effective pressure and the sign of the melt rate. When the melt rate is positive (i.e., melting) there is always a steady state fringe thickness for any effective pressure greater than the critical pressure to form a fringe (i.e. equation 3). When the melt rate is negative (i.e. freezing), however, there is not always a steady state and the fringe may grow with time and without bound. These two possibilities are shown in Figure 7c. For the largest effective pressure $N = 200$ kPa, the melt rate never drops below zero and therefore the fringe grows to a new steady state during the WIS slowdown, which is inconsistent. In the other two cases, however, the melt rate becomes negative and the fringe grows precipitously with time. As the fringe grows, the resistance to sliding must also grow. Thus, it is consistent that the fringe beneath WIS has grown during the slowdown.

The interpretation of active seismic observations

Seismic wave impedance $z = \rho_i c$, the product of density and wave speed, has been found to be correlated with basal seismicity on the Rutford (Smith, 1997, 2006) and Whillans ice streams (Luthra and others, 2016). Impedance variations have historically been inferred to be related to porosity (Blankenship and others, 1986). However, as noted by Smith (1997), in some cases variations in entrained debris may cause similar impedance variations. In light of the proposed connection between rate-weakening friction

and entrained debris, we find this line of reasoning to provide a compelling explanation of the relationship between impedance variations and basal seismicity. We note that in cases of high data quality, seismological investigations using amplitude variation with offset (AVO) may be able to directly resolve the apparent ambiguity between basal debris and low porosity till (Luthra and others, 2016).

CONCLUSIONS

Here, we propose the hypothesis that sediment entrainment is a necessary but not sufficient condition for subglacial shear seismicity in temperate beds of glaciers and ice sheets. We have provided support for this hypothesis using laboratory experiments and simple models. We note that effective pressure and viscous flow impose additional necessary conditions for the occurrence of seismicity. A corollary of our hypothesis is that basal shear seismicity may be used to image active geomorphic processes as well as the processes that govern the strength of the ice–bed interface.

STABILITY ANALYSIS

Governing Equations

We examine the sliding displacement D near a small, potentially seismogenic region of the bed. The approximate momentum balance is (Mitsui and Hirahara, 2001),

$$\tau_B = \tau_D - \frac{kD}{2} - \frac{\nu}{2}\frac{\partial D_\mu}{\partial t} - \eta\frac{\partial D}{\partial t}. \tag{8}$$

where τ_D is the driving stress, $k = \alpha G/R$ is the elastic stiffness of a bedrock obstacle of dimension R with shear modulus G, and α is a geometrical parameter of order unity (Lipovsky and Dunham, 2016). The radiation damping parameter $\eta \equiv G/(2c)$ for shear wave speed c. Viscous displacements D_μ follow

$$\frac{\partial D_\mu}{\partial t} = \frac{k}{\mu}\left(D - D_\mu\right). \tag{9}$$

The parameters that are held fixed in our analysis are listed in Table 2. The linearized effective viscosity μ is chosen to reflect flow around a bedrock obstacle of characteristic dimension R (Kamb, 1970; Meyer and

388 others, 2018a). For reference sliding rate v_0 this results in a strain rate $\sim v_0/R$ and then

$$\mu = A^{-1/n} \left(\frac{v_0}{\epsilon R} \right)^{(1-n)/n} \tag{10}$$

389 where ϵ is the bedrock bump aspect ratio.

390 The basal shear stress τ_B is set by rate and state friction,

$$\frac{\partial \tau_B}{\partial t} = \frac{aN}{V} \frac{\partial V}{\partial t} + \frac{V}{L} \left[\tau - \tau_{ss}(V) \right]. \tag{11}$$

391 Here, a measures the instantaneous shear strength increase upon an increase of the sliding velocity V, N
392 is the effective pressure, L is the state evolution distance, and τ_{ss} is the steady state friction coefficient,

$$\tau_{ss} \equiv N \left[f_0 - (b-a) \log \left(\frac{V}{v_0} \right) \right], \tag{12}$$

393 with state evolution parameter b. The parameters used in this formulation of basal sliding are discussed
394 extensively by Lipovsky and Dunham (2017).

395 Linearization and stability

396 We linearize the four governing equations (Equations 8, 9, 10, and 11) about a reference state of steady
397 sliding at velocity v_0 and bed shear stress $\tau_0 = N f_0$. We examine solutions that are harmonic in time with
398 complex frequency s. Following classical methods (Rice and others, 2001), we then seek unstable, stick-slip
399 type behavior in the form of solutions s with positive real part.

400 The linearized form of the rate and state friction friction law is then

$$\delta\tau = \frac{aN}{s + v_0/L} \left(s - \frac{v_0}{L} \frac{b-a}{a} \right) \frac{s}{v_0} \delta D. \tag{13}$$

401 Perturbed shear stresses and displacementes are denoted with a prefixed delta symbol. The linearized
402 momentum balance for the shear stress perturbation is

$$\delta\tau = -\frac{1}{2} \left[k + 2\eta s + \frac{sk}{s + k/\mu} \right] \delta D \, . \tag{14}$$

Eliminating reference to the perturbed quantities then gives the dispersion relation

$$\begin{aligned} 0 =& s^3 \left(\frac{aN}{v_0} + \eta \right) \\ &+ s^2 \left(\frac{N(a-b)}{L} + \frac{akN}{\mu v_0} + \frac{\eta k}{\mu} + k + \frac{\eta v_0}{L} \right) \\ &+ s \left(\frac{kN(a-b)}{L\mu} + \frac{k^2}{2\mu} + \frac{\eta k v_0}{L\mu} + \frac{k v_0}{L} \right) \\ &+ \frac{k^2 v_0}{2L\mu} \, . \end{aligned} \tag{15}$$

Basal seismicity occurs when solutions s to the dispersion relation have positive real part. This occurs when

$$\frac{N(b-a)}{L} > \left(\frac{aN}{v_0} + \eta \right) \frac{k}{\mu} + k + \frac{\eta v_0}{L}. \tag{16}$$

When $\eta, \ \mu \to \infty$, we recover the quasi-static elastic limit,

$$N \geqslant \frac{kL}{(b-a)} \equiv N_c. \tag{17}$$

Including the effect of radiation damping recovers the limit from Lipovsky and Dunham (2016),

$$\frac{N(b-a)}{L} > k + \frac{\eta v_0}{L}. \tag{18}$$

Neglecting radiation damping but keeping viscosity

$$\frac{N_c}{N} < 1 - \frac{a}{b-a} \frac{L/v_0}{\mu/k}. \tag{19}$$

This condition can then be rearranged to give Equation 4 in the main text. Following Lipovsky and Dunham (2017), the stick-slip recurrence time is proportional to

$$T_r \equiv \frac{a}{b-a} \frac{L}{v_0},$$

which is different from the time scale T_c defined by Lipovsky and Dunham (2017) by a factor of $\sqrt{a/(b-a)}$, a difference that we attribute to the approximate nature of the simplified model presented here. Despite this difference, we nevertheless expect the ratio of the Maxwell time and the recurrence time to be the

nondimensional parameter governing the suppression of seismicity due to viscous flow.

Including viscoelastic and radiation damping effects gives the full stability condition:

$$N > \frac{\mu}{a}\left(1 + \frac{\eta}{\mu} + \frac{\eta v_0}{kL}\right)\left[\frac{1}{v_c} - \frac{1}{v_0}\right]^{-1}. \tag{20}$$

REFERENCES

Acomb LJ, Mickelson DM and Evenson EB (1982) Till stratigraphy and late glacial events in the lake michigan lobe of eastern wisconsin. *Geological Society of America Bulletin*, **93**(4), 289–296

Alley R, Anandakrishnan S, Bentley C and Lord N (1994) A water-piracy hypothesis for the stagnation of Ice Stream C, Antarctica. *Annals of Glaciology*, **20**, 187–194

Alley RB, Blankenship DD, Bentley CR and Rooney S (1986) Deformation of till beneath ice stream b, west antarctica. *Nature*, **322**(6074), 57

Allison KL and Dunham EM (2018) Earthquake cycle simulations with rate-and-state friction and power-law viscoelasticity. *Tectonophysics*, **733**, 232–256

Allstadt K and Malone SD (2014) Swarms of repeating stick-slip icequakes triggered by snow loading at mount rainier volcano. *Journal of Geophysical Research: Earth Surface*, **119**(5), 1180–1203

Anandakrishnan S and Bentley CR (1993) Micro-earthquakes beneath Ice Streams B and C, West Antarctica: observations and implications. *Journal of Glaciology*, **39**(133), 455–462

Aster R and Winberry J (2017) Glacial seismology. *Reports on Progress in Physics*, **80**(12), 126801

Barcheck CG, Tulaczyk S, Schwartz SY, Walter JI and Winberry JP (2018) Implications of basal micro-earthquakes and tremor for ice stream mechanics: Stick-slip basal sliding and till erosion. *Earth and Planetary Science Letters*, **486**, 54–60

Barnes P, Tabor D and Walker J (1971) The friction and creep of polycrystalline ice. *Proceedings of the Royal Society of London. A. Mathematical and Physical Sciences*, **324**(1557), 127–155

Beem L, Tulaczyk S, King M, Bougamont M, Fricker H and Christoffersen P (2014) Variable deceleration of Whillans Ice Stream, West Antarctica. *Journal of Geophysical Research: Earth Surface*, **119**(2), 212–224

Bindschadler RA, King MA, Alley RB, Anandakrishnan S and Padman L (2003) Tidally controlled stick-slip discharge of a west antarctic ice. *Science*, **301**(5636), 1087–1089

Blake W, Fischer UH, Bentley C and Clarke GK (1994) Instruments and methods: Direct measurement of sliding at the glacier bed. *Journal of Glaciology*, **40**(136), 595–599

Blankenship DD, Bentley CR, Rooney S and Alley RB (1986) Seismic measurements reveal a saturated porous layer beneath an active Antarctic ice stream. *Nature*, **322**(6074), 54

Canassy PD, Röösli C and Walter F (2016) Seasonal variations of glacier seismicity at the tongue of rhonegletscher (switzerland) with a focus on basal icequakes. *Journal of Glaciology*, **62**(231), 18–30

Clarke GK (2005) Subglacial processes. *Annu. Rev. Earth Planet. Sci.*, **33**, 247–276

Dash J, Rempel A and Wettlaufer J (2006) The physics of premelted ice and its geophysical consequences. *Reviews of modern physics*, **78**(3), 695

Dieterich JH (1978) Time-dependent friction and the mechanics of stick-slip. In *Rock Friction and Earthquake Prediction*, 790–806, Springer

Dieterich JH (2007) Applications of rate-and state-dependent friction to models of fault slip and earthquake occurrence. In G Schubert (ed.), *Treatise on Geophysics*, volume 4, Elsevier (Oxford)

Emerson L and Rempel A (2007) Thresholds in the sliding resistance of simulated basal ice. *The Cryosphere Discussions*, **1**(1), 99–122

Goldberg D, Schoof C and Sergienko O (2014) Stick-slip motion of an Antarctic Ice Stream: The effects of viscoelasticity. *Journal of Geophysical Research: Earth Surface*, **119**(7), 1564–1580

Helmstetter A, Nicolas B, Comon P and Gay M (2015) Basal icequakes recorded beneath an alpine glacier (glacier d'argentière, mont blanc, france): Evidence for stick-slip motion? *Journal of Geophysical Research: Earth Surface*, **120**(3), 379–401

Hosler CL, Jensen D and Goldshlak L (1957) On the aggregation of ice crystals to form snow. *Journal of Meteorology*, **14**(5), 415–420

Iverson NR (2010) Shear resistance and continuity of subglacial till: hydrology rules. *J. Glaciol.*, **56**(200), 1104–1114 (doi: 10.3189/002214311796406220)

Kamb B (1970) Sliding motion of glaciers: theory and observation. *Reviews of Geophysics*, **8**(4), 673–728

Kamb B (2001) Basal zone of the West Antarctic ice streams and its role in lubrication of their rapid motion. *The West Antarctic ice sheet: behavior and environment*, 157–199

Kennedy F, Schulson E and Jones D (2000) The friction of ice on ice at low sliding velocities. *Philosophical Magazine A*, **80**(5), 1093–1110

Leeman J, Scuderi MM, Marone C and Saffer D (2015) Stiffness evolution of granular layers and the origin of repetitive, slow, stick-slip frictional sliding. *Granular Matter*, **17**(4), 447–457

Linker M and Dieterich J (1992) Effects of variable normal stress on rock friction: Observations and constitutive equations. *Journal of Geophysical Research: Solid Earth*, **97**(B4), 4923–4940

Lipovsky BP and Dunham EM (2016) Tremor during ice-stream stick slip. *The Cryosphere*, **10**(1), 385–399

Lipovsky BP and Dunham EM (2017) Slow-slip events on the Whillans Ice Plain, Antarctica, described using rate-and-state friction as an ice stream sliding law. *Journal of Geophysical Research: Earth Surface*, **122**(4), 973–1003

Lovell H, Fleming EJ, Benn DI, Hubbard B, Lukas S, Rea BR, Noormets R and Flink AE (2015) Debris entrainment and landform genesis during tidewater glacier surges. *Journal of Geophysical Research: Earth Surface*, **120**(8), 1574–1595

Luthra T, Anandakrishnan S, Winberry JP, Alley RB and Holschuh N (2016) Basal characteristics of the main sticky spot on the ice plain of Whillans Ice Stream, Antarctica. *Earth and Planetary Science Letters*, **440**, 12–19

Maeno N and Arakawa M (2004) Adhesion shear theory of ice friction at low sliding velocities, combined with ice sintering. *Journal of Applied Physics*, **95**(1), 134–139

Marone C (1998) Laboratory-derived friction laws and their application to seismic faulting. *Annual Review of Earth and Planetary Sciences*, **26**(1), 643–696

McCarthy C, Savage H and Nettles M (2017) Temperature dependence of ice-on-rock friction at realistic glacier conditions. *Phil. Trans. R. Soc. A*, **375**(2086), 20150348

Meyer CR and Minchew BM (2018) Temperate ice in the shear margins of the antarctic ice sheet: Controlling processes and preliminary locations. *Earth and Planetary Science Letters*, **498**, 17–26

Meyer CR, Downey AS and Rempel AW (2018a) Freeze-on limits bed strength beneath sliding glaciers. *Nature communications*, **9**(1), 3242

Meyer CR, Yehya A, Minchew B and Rice JR (2018b) A model for the downstream evolution of temperate ice and subglacial hydrology along ice stream shear margins. *Journal of Geophysical Research: Earth Surface*, **123**(8), 1682–1698

Mitsui N and Hirahara K (2001) Viscoelastic simulation of earthquake cycle using a simple spring-dashpot-mass system with a friction law. *Geophysical research letters*, **28**(23), 4391–4394

Moore PL (2014) Deformation of debris-ice mixtures. *Reviews of Geophysics*, **52**(3), 435–467

Moore PL and Iverson NR (2002) Slow episodic shear of granular materials regulated by dilatant strengthening. *Geology*, **30**(9), 843–846

Moore PL, Iverson NR and Cohen D (2010) Conditions for thrust faulting in a glacier. *Journal of Geophysical Research: Earth Surface*, **115**(F2)

Morlighem M, Seroussi H, Larour E and Rignot E (2013) Inversion of basal friction in antarctica using exact and incomplete adjoints of a higher-order model. *Journal of Geophysical Research: Earth Surface*, **118**(3), 1746–1753

Oksanen P and Keinonen J (1982) The mechanism of friction of ice. *Wear*, **78**(3), 315–324

O'Neill K and Miller RD (1985) Exploration of a rigid ice model of frost heave. *Water Resources Research*, **21**(3), 281–296

Podolskiy EA and Walter F (2016) Cryoseismology. *Reviews of geophysics*, **54**(4), 708–758

Pratt MJ, Winberry JP, Wiens DA, Anandakrishnan S and Alley RB (2014) Seismic and geodetic evidence for grounding-line control of whillans ice stream stick-slip events. *Journal of Geophysical Research: Earth Surface*, **119**(2), 333–348

Rathbun AP, Marone C, Alley RB and Anandakrishnan S (2008) Laboratory study of the frictional rheology of sheared till. *Journal of Geophysical Research: Earth Surface*, **113**(F2)

Rempel A (2007) Formation of ice lenses and frost heave. *Journal of Geophysical Research: Earth Surface*, **112**(F2)

Rempel A (2008) A theory for ice-till interactions and sediment entrainment beneath glaciers. *Journal of Geophysical Research: Earth Surface*, **113**(F1)

Rempel A, Wettlaufer J and Worster M (2001) Interfacial premelting and the thermomolecular force: thermodynamic buoyancy. *Physical review letters*, **87**(8), 088501

Rempel AW (2009a) Effective stress profiles and seepage flows beneath glaciers and ice sheets. *Journal of Glaciology*, **55**(191), 431–443

Rempel AW (2009b) Transient effective stress variations forced by changes in conduit pressure beneath glaciers and ice sheets. *Annals of Glaciology*, **50**(52), 61–66

Rempel AW and Rice JR (2006) Thermal pressurization and onset of melting in fault zones. *Journal of Geophysical Research: Solid Earth*, **111**(B9)

Rempel AW, Wettlaufer J and Worster MG (2004) Premelting dynamics in a continuum model of frost heave. *Journal of Fluid Mechanics*, **498**, 227–244

Rice J and Ruina AL (1983) Stability of steady frictional slipping. *Journal of applied mechanics*, **50**(2), 343–349

Rice JR (2006) Heating and weakening of faults during earthquake slip. *Journal of Geophysical Research: Solid Earth*, **111**(B5)

Rice JR, Lapusta N and Ranjith K (2001) Rate and state dependent friction and the stability of sliding between elastically deformable solids. *Journal of the Mechanics and Physics of Solids*, **49**(9), 1865–1898

Robin GdQ (1976) Is the basal ice of a temperate glacier at the pressure melting point? *Journal of Glaciology*, **16**(74), 183–196

Roeoesli C, Helmstetter A, Walter F and Kissling E (2016) Meltwater influences on deep stick-slip icequakes near the base of the greenland ice sheet. *Journal of Geophysical Research: Earth Surface*, **121**(2), 223–240

Sammis CG and Ben-Zion Y (2008) Mechanics of grain-size reduction in fault zones. *Journal of Geophysical Research: Solid Earth*, **113**(B2)

Scholz C and Engelder J (1976) The role of asperity indentation and ploughing in rock friction—i: Asperity creep and stick-slip. In *International Journal of Rock Mechanics and Mining Sciences & Geomechanics Abstracts*, volume 13, 149–154, Elsevier

Scholz CH (1998) Earthquakes and friction laws. *Nature*, **391**(6662), 37

Schoof C (2005) The effect of cavitation on glacier sliding. In *Proceedings of the Royal Society of London A: Mathematical, Physical and Engineering Sciences*, volume 461(2055), 609–627, The Royal Society

Selvadurai A, Selvadurai P and Suvorov A (2018) Contact mechanics of a dilatant region located at a compressed elastic interface. *International Journal of Engineering Science*, **133**, 144–168

Smith A (1997) Basal conditions on Rutford ice stream, West Antarctica, from seismic observations. *Journal of Geophysical Research: Solid Earth*, **102**(B1), 543–552

Smith A (2006) Microearthquakes and subglacial conditions. *Geophysical Research Letters*, **33**(24)

Smith E, Smith A, White R, Brisbourne A and Pritchard H (2015) Mapping the ice-bed interface characteristics of rutford ice stream, west antarctica, using microseismicity. *Journal of Geophysical Research: Earth Surface*, **120**(9), 1881–1894

Thomason JF and Iverson NR (2008) A laboratory study of particle ploughing and pore-pressure feedback: a velocity-weakening mechanism for soft glacier beds. *J. Glaciol.*, **54**(184), 169–181 (doi: 10.3189/002214308784409008)

Tulaczyk SM, Scherer RP and Clark CD (2001) A ploughing model for the origin of weak tills beneath ice streams: a qualitative treatment. *Quaternary International*, **86**(1), 59–70

van der Veen CJ and Whillans I (1989) Force budget: I. theory and numerical methods. *Journal of Glaciology*, **35**(119), 53–60

Viesca RC and Garagash DI (2015) Ubiquitous weakening of faults due to thermal pressurization. *Nature Geoscience*, **8**(11), 875

Wiens DA, Anandakrishnan S, Winberry JP and King MA (2008) Simultaneous teleseismic and geodetic observations of the stick–slip motion of an antarctic ice stream. *Nature*, **453**(7196), 770

Winberry JP, Anandakrishnan S, Wiens DA, Alley RB and Christianson K (2011) Dynamics of stick–slip motion, whillans ice stream, antarctica. *Earth and Planetary Science Letters*, **305**(3-4), 283–289

Winberry JP, Anandakrishnan S, Wiens DA and Alley RB (2013) Nucleation and seismic tremor associated with the glacial earthquakes of whillans ice stream, antarctica. *Geophysical Research Letters*, **40**(2), 312–315

Zoet L, Carpenter B, Scuderi M, Alley R, Anandakrishnan S, Marone C and Jackson M (2013) The effects of entrained debris on the basal sliding stability of a glacier. *Journal of Geophysical Research: Earth Surface*, **118**(2), 656–666

Zoet LK and Iverson NR (2015) Experimental determination of a double-valued drag relationship for glacier sliding. *J. Glac.*, **61**(225), 1–7

Zoet LK and Iverson NR (2016) Rate-weakening drag during glacier sliding. *Journal of Geophysical Research: Earth Surface*, **121**(7), 1206–1217

Zoet LK and Iverson NR (2018) A healing mechanism for stick-slip of glaciers. *Geology*, **46**(9), 807–810

Zoet LK, Anandakrishnan S, Alley RB, Nyblade AA and Wiens DA (2012) Motion of an antarctic glacier by repeated tidally modulated earthquakes. *Nature Geoscience*, **5**(9), 623